ORIGINAL ARTICLE

Rapid displacement determination with a stand-alone multi-GNSS receiver: GPS, Beidou, GLONASS, and Galileo

Ke Su[1,2] · Shuanggen Jin[1,3] · Yulong Ge[2,4]

Abstract

Global Navigation Satellite System (GNSS) is an effective tool to retrieve displacement with high precision. Relative positioning and precise point positioning (PPP) are two basic techniques. We present a multi-GNSS dynamic PPP model considering the parameters of velocity and acceleration to determine high-precision displacement rapidly. The performance evaluations of dynamic PPP are conducted in terms of convergence time and positioning repeatability. The mean convergence time of GPS-only, Beidou-only, GPS + Beidou, GPS + GLONASS, GPS + Galileo, and quad-constellation dynamic PPP are 49.4, 104.5, 45.3, 39.9, 47.3, and 35.1 s, respectively. The Beidou-only dynamic PPP has poorer positioning repeatability than the GPS-only solution and the integration of multi-GNSS will enhance the positioning repeatability. The usability of multi-GNSS dynamic PPP for kinematic application is demonstrated by a vehicle-borne kinematic experiment and seismic waves capture data at station LASA during the 2015 M_w 7.8 Nepal earthquake. The dynamic PPP for the kinematic test will be improved in terms of positioning precision with more GNSS constellations and does not suffer the long convergence time compared with kinematic solutions.

Keywords Multi-GNSS · Dynamic PPP · Convergence time · Positioning precision

Introduction

With the rapid development of the Global Navigation Satellite System (GNSS), an increasing number of tracking stations and constellations is constructed. The emerging navigation satellite systems are offering the space-based positioning, navigation, and timing (PNT) services. As the first space-based radio-navigation system, GPS has made remarkable contributions to the scientific application and engineering services (Li et al. 2013; Paul et al. 2009; Jin et al. 2016). China's Beidou Navigation Satellite System set

out to provide positioning services and regional navigation and is intended to enable full global coverage by 2020 (Yang et al. 2014). The GLONASS was fully recovered by October 2011, and is operating at full capability with 24 satellites in orbits and offering global positioning service (Wei et al. 2015). The Galileo is in the transition phase to full operational capability and started offering the initial operational capability on December 15, 2016 and expected to consist of 30 available satellites once fully deployed (Li et al. 2018). With the increasing number of available satellites, the integration of different GNSS constellations provides a considerable opportunity to enhance PNT performance and has great potential to provide reliable and precise services to GNSS users (Montenbruck et al. 2014; Jin et al. 2015, Su et al. 2019).

Precise displacement measurement is significant for dynamic applications. Nowadays, there are two basic approaches for precise displacement determination: relative kinematic positioning and kinematic precise point positioning (PPP) (Lambiel and Delaloye 2004; Zumberge et al. 1997). In relative kinematic positioning, one or more reference stations can be utilized to recover the integer feature of double-differenced ambiguities. Consequently, the high

✉ Shuanggen Jin
  sgjin@shao.ac.cn; sg.jin@yahoo.com

[1] Shanghai Astronomical Observatory, Chinese Academy of Sciences, Shanghai 200030, China

[2] University of Chinese Academy of Sciences, Beijing 100049, China

[3] School of Remote Sensing and Geomatics Engineering, Nanjing University of Information Science and Technology, Nanjing 210044, China

[4] National Time Service Center, Chinese Academy of Sciences, Xi'an 710600, China

positioning accuracy of few centimeters can be guaranteed when the ambiguities are fixed. However, the difficulties introduced by the ionospheric delay in the case of medium-range or long-range applications cannot be neglected. Hence, the single baseline real-time kinematic (RTK) is limited to short-range baseline, generally less than 15 km (Guo et al. 2011). For network relative positioning technique, it needs many stations for simultaneous observations and is complicated by the need to assign baselines or overlapping sub-networks. Intermittent station dropouts will complicate the network-based relative positioning. In additional, relative positioning only provides a relative position and relies on the reference station. When the reference station is far or even undergoes a displacement, the absolute displacements within the global reference frame are not available anymore.

Alternatively, when precise satellite orbit and clock products and high-rate GNSS observations are available, PPP can provide absolute displacements in a global reference frame with a single receiver. The products can be obtained through the multi-GNSS experiment (MGEX) project set by the International GNSS Service (IGS) (Rizos et al. 2013). Tegedor et al. (2014) analyzed the performance of the quad-constellation PPP solutions by the MGEX products for the first time. PPP does not need the reference stations compared to relative positioning. Whereas the long convergence time is the major problem of PPP, it will take up 30–60 min before the positioning errors converge (Li et al. 2015). It still takes 15–20 min to converge when applying the ambiguity resolution technology (Ge et al. 2008). Furthermore, repeated re-initialization or even non-convergent solutions when cycle slip occurred can lead to gross errors in the PPP solution (Guo and Zhang 2014).

In addition, time-differenced carrier-phase measurement (TDCP) is another method to measure displacement without fixing the ambiguity (Wendel et al. 2006). In TDCP, the epoch-by-epoch displacements, integrated by velocities, will be noisy and drift due to the high-frequency noises from epoch differencing. Colosimo et al. (2011) presented a variometric approach to determine displacement by the single integration of delta positions. The derived displacements will be drifting and can be at a few centimeters level after linear trend removal (Branzanti et al. 2013). Tu (2013) proposed the approach to rapidly determine displacements with GPS observations using PPP velocity estimation. The time series of velocities are integrated into displacements without drifting.

We present a GPS + Beidou + GLONASS + Galileo dynamic PPP model for rapid displacement determination with observations from quad-constellations based on the PPP velocity estimation approach. The multi-GNSS dynamic PPP additionally estimates the parameters of velocity and acceleration in an epoch. The displacement is determined by integrating the velocity and acceleration parameters

between two adjacent epochs. The performance of dynamic PPP is assessed in terms of convergence time and positioning repeatability through 1 Hz static data sets provided by MGEX. The benefits of dynamic PPP for kinematic application are also demonstrated. A kinematic experiment in Beijing on March 30, 2018 is conducted, and seismic waves of station LASA from the Beidou Experiment Tracking Station (BETS), induced by the 2015 M_w 7.8 Nepal earthquake event, are also analyzed by different dynamic PPP solutions.

Displacement determination by dynamic PPP

The GNSS undifferenced (UD) pseudorange and carrier-phase observations for the observation between the receiver and satellite can be expressed as follows (Leick et al. 2015):

$$p_{r,j}^s = \rho_r^s + c(dt_r - dt^s) + T_r^s + I_{r,j}^s + c(d_{r,j} + d_j^s) + \varepsilon_p \tag{1}$$

$$\varphi_{r,j}^s = \rho_r^s + c(dt_r - dt^s) + T_r^s - I_{r,j}^s + \lambda_j w_r^s + \lambda_j N_{r,j}^s + \lambda_j(b_{r,j} - b_j^s) + \varepsilon_\varphi, \tag{2}$$

where the superscript s denotes a GNSS satellite; the subscript r and j denote the receiver and the frequency; $p_{r,j}^s$ denotes the observed pseudorange on jth frequency in meters; $\varphi_{r,j}^s$ is the corresponding carrier phase; ρ_r^s denotes the geometrical range from phase centers of the satellite to receiver antennas at the signal transmitting and receive time in meters; c denotes the vacuum speed of light in meters per second; dt_r is the receiver clock offset in seconds; dt^s is the satellite clock offset in seconds; T_r^s is the slant tropospheric delay in meters; $I_{r,j}^s$ is the ionospheric delay on jth frequency in meters; $d_{r,j}$ and d_j^s are the code biases of the receiver and the satellite in seconds; λ_j is the wavelength of carrier phase on the jth frequency in meters; w_r^s is the phase wind-up delay in cycles; $N_{r,j}^s$ is the integer ambiguity on the jth frequency in cycles; $b_{r,j}$ and b_j^s are the uncalibrated phase delays (UPDs) for receiver and satellites in cycles, respectively. ε_p and ε_φ are the pseudorange and carrier-phase observation noises including multipath in meters, respectively.

The linear combinations of observations at different frequencies can eliminate the first order of the ionospheric delays, for instance, the ionospheric-free (IF) combination, which can be written as follows (Kouba and Heroux 2001):

$$p_{r,IF}^s = (f_1^2 \cdot p_{r,1}^s - f_2^2 \cdot p_{r,2}^s)/(f_1^2 - f_2^2) \tag{3}$$

$$\varphi_{r,IF}^s = (f_1^2 \cdot \varphi_{r,1}^s - f_2^2 \cdot \varphi_{r,2}^s)/(f_1^2 - f_2^2). \tag{4}$$

The tropospheric delay cannot be eliminated by the combination of the observations. The dry component of tropospheric delay is generally corrected with the a priori model

whereas the residual wet part is estimated from the observations (Davis et al. 1985). In addition, some other error mitigations, including the phase center variations and offsets, tidal loading deduced displacements, the relativistic effects, and earth rotation also need to be corrected according to the models in the International Earth Rotation and Reference Systems Service (IERS) Convention 2010 (Petit and Luzum 2010), although they are not included in the above equations. By convention, the precise satellite clock correction is associated with the IF combination. Hence, the satellite code biases can be mitigated by forming IF combinations (Guo et al. 2015). The UPDs in the carrier phase will be mapped into ambiguities, and thus, the ambiguities are estimated as float values.

When the terms mentioned above are removed, the pseudorange and carrier phase can be further simplified as follows:

$$p_{r,IF}^{s} = \bar{\rho}_{r}^{s} + cdt_{r} + M_{r}^{s}T_{r} + cd_{r,IF} + \varepsilon_{p,IF} \tag{5}$$

$$\varphi_{r,IF}^{s} = \bar{\rho}_{r}^{s} + cdt_{r} + M_{r}^{s}T_{r} + \lambda_{IF}\bar{N}_{r,IF}^{s} + \varepsilon_{\varphi,IF}, \tag{6}$$

where $\bar{\rho}_{r}^{s}$ is ρ_{r}^{s} plus other error sources; M_{r}^{s} denotes the mapping function of wet tropospheric delays; T_{r} denotes the zenith wet tropospheric delay; $\bar{N}_{r,j}^{s}$ denotes the float ambiguities.

For multi-GNSS positioning, each navigation system has its own spatial reference scale, timescale, and signal structure. Although the reference system of precise orbit and clock products is the same, one still has to consider the influence of hardware biases in both receivers and satellites, which exist due to differences of signals. The hardware biases will be absorbed in receiver clock parameters for each navigation system. We introduce the system time difference parameters for each satellite system with respect to GPS system time, and then, the IF observation for GPS, Beidou, GLONASS, and Galileo can be written as follows:

$$p_{r,IF}^{G,s} = \bar{\rho}_{r}^{G,s} + cd\tilde{t}_{r}^{G} + M_{r}^{G,s}T_{r} + \varepsilon_{p,IF}^{G,s} \tag{7}$$

$$\varphi_{r,IF}^{G,s} = \bar{\rho}_{r}^{G,s} + cd\tilde{t}_{r}^{G} + M_{r}^{G,s}T_{r} + \lambda_{r,IF}^{G}\tilde{N}_{r,IF}^{G,s} + \varepsilon_{\varphi,IF}^{G,s} \tag{8}$$

$$p_{r,IF}^{C,s} = \bar{\rho}_{r}^{C,s} + cd\tilde{t}_{r}^{G} + cdt_{G}^{C} + M_{r}^{C,s}T_{r} + \varepsilon_{p,IF}^{C,s} \tag{9}$$

$$\varphi_{r,IF}^{C,s} = \bar{\rho}_{r}^{C,s} + cd\tilde{t}_{r}^{G} + cdt_{G}^{C} + M_{r}^{C,s}T_{r} + \lambda_{r,IF}^{C}\tilde{N}_{r,IF}^{C,s} + \varepsilon_{\varphi,IF}^{C,s} \tag{10}$$

$$p_{r,IF}^{R,s} = \bar{\rho}_{r}^{R,s} + cd\tilde{t}_{r}^{G} + cdt_{G}^{R,s} + M_{r}^{R,s}T_{r} + \varepsilon_{p,IF}^{R,s} \tag{11}$$

$$\varphi_{r,IF}^{R,s} = \bar{\rho}_{r}^{R,s} + cd\tilde{t}_{r}^{G} + cdt_{G}^{R,s} + M_{r}^{R,s}T_{r} + \lambda_{r,IF}^{R}\tilde{N}_{r,IF}^{R,s} + \varepsilon_{\varphi,IF}^{R,s} \tag{12}$$

$$p_{r,IF}^{E,s} = \bar{\rho}_{r}^{E,s} + cd\tilde{t}_{r}^{G} + cdt_{G}^{E} + M_{r}^{E,s}T_{r} + \varepsilon_{p,IF}^{E,s} \tag{13}$$

$$\varphi_{r,IF}^{E,s} = \bar{\rho}_{r}^{E,s} + cd\tilde{t}_{r}^{G} + cdt_{G}^{E} + M_{r}^{E,s}T_{r} + \lambda_{r,IF}^{E}\tilde{N}_{r,IF}^{E,s} + \varepsilon_{\varphi,IF}^{E,s}, \tag{14}$$

where G, C, R and E represent the GPS, Beidou, GLONASS, and Galileo satellite; cdt_{G}^{C}, $cdt_{G}^{R,s}$, and cdt_{G}^{E} are the system time difference parameters; $cd\tilde{t}_{r}^{G}$ and $\tilde{N}_{r,IF}^{s}$ are the reparameterized GPS receiver clock offset and ambiguity parameter, respectively, which are as $cd\tilde{t}_{r}^{G}=cdt_{r}^{G} + cd_{r,IF}^{G}$ and $\tilde{N}_{r,IF}^{s}=\bar{N}_{r,IF}^{s} - cd_{r,IF}^{G}$. The inter-system biases (ISBs) of different constellations are estimated in the combined processing of multi-GNSS observations. The biases for the GLONASS satellites are different and called the inter-frequency biases (IFBs). The multi-GNSS dynamic PPP estimates the parameters of displacement, velocity and acceleration simultaneously in an epoch. Hence, the estimated parameters in multi-GNSS dynamic PPP include receiver displacement, velocity, acceleration, zenith wet tropospheric delay, GPS receiver clock offset, ISB parameters for Beidou and Galileo, IFB parameters for each GLONASS satellite, and float ambiguities.

The dynamic PPP model assumes that the receiver is in a steady acceleration state between two adjacent epochs, and the variation of displacement, velocity, and acceleration is random. Hence, the time interval of observation data cannot be too long, generally less than 3 s (Yang et al. 2001). The Kalman filter is employed for the multi-GNSS PPP processing (Kalman 1960). The state transition and process noise matrices can be determined according to Tu (2013). The design matrix A and the state matrix X in the Kalman filter can be expressed as follows:

$$A = \begin{bmatrix} e^{G,s} & 0 & 0 & M_{r}^{G,s} & -1 & 0 & 0 & 0 & \lambda_{r,IF}^{G} & 0 & 0 & 0 \\ e^{G,s} & 0 & 0 & M_{r}^{G,s} & -1 & 0 & 0 & 0 & 0 & 0 & 0 & 0 \\ e^{C,s} & 0 & 0 & M_{r}^{C,s} & -1 & -1 & 0 & 0 & 0 & \lambda_{r,IF}^{C} & 0 & 0 \\ e^{C,s} & 0 & 0 & M_{r}^{C,s} & -1 & -1 & 0 & 0 & 0 & 0 & 0 & 0 \\ e^{R,s} & 0 & 0 & M_{r}^{R,s} & -1 & -1 & -1 & 0 & 0 & 0 & \lambda_{r,IF}^{R} & 0 \\ e^{R,s} & 0 & 0 & M_{r}^{R,s} & -1 & -1 & -1 & 0 & 0 & 0 & 0 & 0 \\ e^{E,s} & 0 & 0 & M_{r}^{E,s} & -1 & -1 & -1 & -1 & 0 & 0 & 0 & \lambda_{r,IF}^{E} \\ e^{E,s} & 0 & 0 & M_{r}^{R,s} & -1 & -1 & -1 & -1 & 0 & 0 & 0 & 0 \end{bmatrix} \tag{15}$$

$$X = [\, s_{r} \quad v_{r} \quad a_{r} \quad T_{r} \quad cd\tilde{t}_{r}^{G} \quad cdt_{G}^{C} \quad cdt_{G}^{R,s} \quad cdt_{G}^{E} \quad \tilde{N}_{r,IF}^{G,s} \quad \tilde{N}_{r,IF}^{C,s} \quad \tilde{N}_{r,IF}^{R,s} \quad \tilde{N}_{r,IF}^{C,s} \,], \tag{16}$$

where e is the unit vector from satellite to receiver; s_{r}, v_{r}, and a_{r} denote the parameters of the receiver displacement, velocity, and acceleration, respectively.

In multi-GNSS dynamic PPP, the estimated displacement in the equation is not directly used. Alternatively,

the estimated velocity and acceleration is integrated to displacement, which can be expressed as follows:

$$[s_r{}']_k = \sum_{i=k_0}^{i=k} \left([v_r]_i \cdot \tau + \frac{1}{2}[a_r]_i \cdot \tau^2 \right), \tag{17}$$

where $s_r{}'$ are the integrated displacements and k_0 is the beginning epoch.

Data processing and performance analysis

The section begins by introducing the data processing strategy of dynamic PPP solutions used in this study. A total of 840 sets of results are analyzed to get a statistical conclusion. The performance of dynamic PPP is evaluated in terms of convergence time and positioning repeatability.

Data processing strategy

Table 1 summarizes our multi-GNSS dynamic PPP processing strategy in detail. The static data sets with quad-constellations of the MGEX project set by International GNSS Service (IGS) are utilized. The coordinates of the stations are provided by IGS daily estimates. The processing results of IGS for selected data sets refer to "IGS14". The IF observations from GPS L1/L2, Beidou B1/B2, GLONASS G1/G2, and Galileo E1/E5a signals are used and have a sampling interval of 1 s. The satellite elevation mask angle is 10°. Multi-constellation precise satellite orbit and clock products provided by Deutsches GeoForschungsZentrum (GFZ) are adopted for multi-GNSS dynamic PPP processing. The orbit and clock products have a sampling interval of 5 min and 30 s, respectively. The antenna file data generated by IGS are utilized to correct the GNSS satellite phase center offset (PCO). The tropospheric delay for its dry component is corrected with the modified Hopfield model based on the GPT2 model (Hopfield 1969; Lagler et al. 2013). The Vienna mapping functions (VMF) are used correspondingly to acquire the mapping functions of both dry and wet parts according to the elevation angle of each satellite (Boehm and Schuh 2004).

In the Kalman filter for dynamic PPP processing, the dynamic noises q_a are set to 0.01 m s$^{-5/2}$ for the static data sets. The tropospheric zenith wet delay (ZWD) is estimated as a random walk process and the receiver clock is estimated as white noises. The ambiguities are estimated as constant for each epoch. The set of spectral density values for the ZWD, the receiver clock offset, and ISB or IFB parameters are 10^{-9}, 10^5, and 10^{-7} m^2/s, respectively. The code observation precision of GPS and GLONASS is set to 0.3 m and the phase observation precision is 0.003 m. The code observation precision for Beidou and Galileo is set to 0.6 m and the phase observation is 0.004 m. The multi-GNSS positioning

Table 1 Multi-GNSS dynamic PPP data processing strategy

Items	Strategies
Estimator	One common Kalman filter
Observations	IF observation; GPS + Beidou + GLONASS + Galileo
Signal selection	GPS L1/L2; Beidou B1/B2; GLONASS G1/G2; Galileo E1/E5a
Sampling rate	1 s
Elevation cut-off	10°
Observation weight	Elevation weight [sin(el)]
Satellite satellites	Fixed by GFZ precise orbit products
Satellite clock	Fixed by GFZ precise clock products
Earth rotation parameter	Fixed (Petit and Luzum 2010)
Relativistic effect	Corrected (Kouba 2009)
Phase wind-up effect	Corrected (Wu et al. 1992)
Tide effect	Solid Earth, pole, and ocean tide (Petit and Luzum 2010)
Satellite antenna	MGEX and IGS values (Petit and Luzum 2010)
Receiver antenna	Corrected (Petit and Luzum 2010)
Station displacements	Estimated in dynamic mode (kinematic mode as a comparison (100 m^2/s))
Station velocities and accelerations	Estimated in dynamic mode (0.01 m s$^{-5/2}$)
Ambiguities	Estimated as constant
Tropospheric delay	Modified Hopfield for dry part and estimated for wet part (10^{-9} m^2/s) (Su and Jin 2018)
Ionospheric delay	Eliminated first order by IF observations
Receiver clock	Estimated as white noises (10^5 m^2/s)
ISB or IFB	Estimated, GPS as a reference (10^{-7} m^2/s)

software was developed by the authors for multi-GNSS PPP processing.

Performance analysis versus kinematic PPP

The positioning performance of dynamic PPP is assessed by multi-GNSS datasets, which are collected and used for numerical analysis at seven stations on February 1–15, 2018. Figure 1 shows the geographical distribution of the selective MGEX stations. All stations can observe GPS, Beidou, GLONASS, and Galileo constellations with multi-GNSS receivers. At least five satellites of each constellation can be observed. The data sets are processed in six constellation combination, i.e., GPS-only (*G*), Beidou-only (*C*),

GPS + Beidou (*GC*), GPS + GLONASS (*GR*), GPS + Galileo (*GE*), and GPS + Beidou + GLONASS + Galileo (*GCRE*).

Taking the quad-constellation station JFNG (China, 30.52°N, 114.49°E) as an example, the data set at JFNG from 00:00 to 03:00 on February 1, 2018 is processed in six different constellation combinations as an example. The performance of kinematic PPP is also analyzed for a comparison. A spectral density of 100 m^2/s for the station coordinate is set in kinematic PPP. Figure 2 shows the velocity and acceleration errors based on six processing cases for dynamic PPP. The errors values are shifted by the same account to avoid overlapping (same operation in Figs. 3, 8, 10). The high accuracy of velocity and acceleration in dynamic PPP can be achieved in a short time as seen in the figure. Table 2 shows the root-mean-square (RMS) values in the north, east, and up velocity and acceleration directions as well as the three-dimension (3-D) values. The RMS is computed based on the errors of the 3 h session solution. It is observed that the GPS-only velocity and acceleration

errors are little more stable than the Beidou-only ones. By combining with Beidou, GLONASS, or Galileo, the dual-constellation dynamic PPP solution is slightly better.

Figure 3 shows the comparison of displacements for 3 h interval at JFNG by kinematic PPP and dynamic PPP based on six processing cases. The left panels show the kinematic PPP results and the right side ones show the dynamic PPP solution. Compared with the kinematic PPP, we can clear see that the dynamic PPP can quickly recover the true displacement. The initial velocity and acceleration errors only cause a system offset to the recovered displacement, but show no effect on the variation of displacement.

The standard deviation (STD) is utilized to indicate the positioning repeatability and assess the performance of displacement variation. Table 3 provides STD statistics in the north, east, and up components as well as STD for the 3-D displacements for both kinematic and dynamic PPP solutions. The STD computations for both kinematic and dynamic solutions are based on the solution errors of the last 2 h where the positioning error of kinematic PPP has converged. In conjunction with the results of Table 2, it is obvious that the multi-constellation combination can improve the precision of the displacement variation of dynamic PPP. The dynamic noises cause the inconsistency of displacements directly derived from kinematic PPP and the integrated displacements in dynamic PPP. In kinematic PPP, the coordinate parameters and ambiguity parameters are correlated, so that it needs a convergent solution to solve the problem of unconverged ambiguities. In dynamic PPP, the velocity and acceleration parameters just depend on the state equation, so that the integrated displacements can be accurately estimated in a short time.

Figure 4 provides the number of satellites and position dilution of precision (PDOP) for the six processing cases. Because the orbits of Beidou geostationary earth orbit (GEO) satellites are distributed in the south of station JFNG,
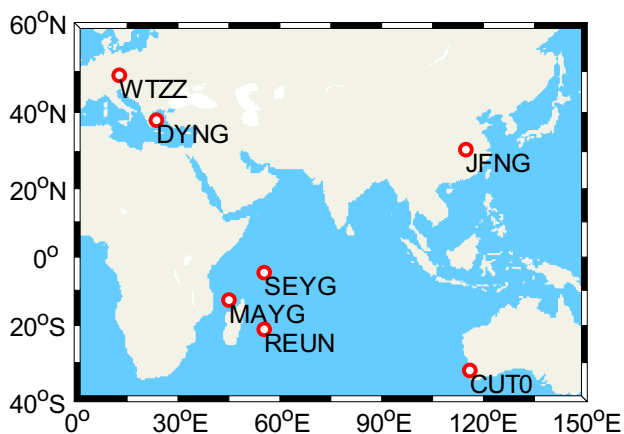

Fig. 1 Geographical distribution of the selective MGEX stations

Fig. 2 Dynamic PPP velocity and acceleration errors at JFNG for six different processing cases. The left panels show the time series of velocity, and the right ones show the time series of acceleration. The abbreviations *G, C, R,* and *E* denote GPS, Beidou, GLONASS, and Galileo, respectively
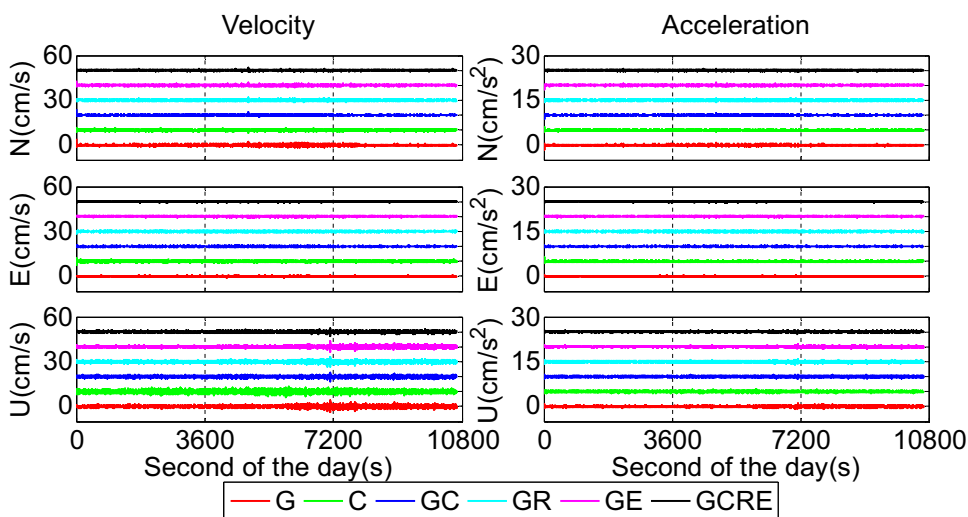
Fig. 3 Displacements for 3 h interval at JFNG. The left panels show the time series of kinematic PPP solution; the right ones show the time series of dynamic PPP solution
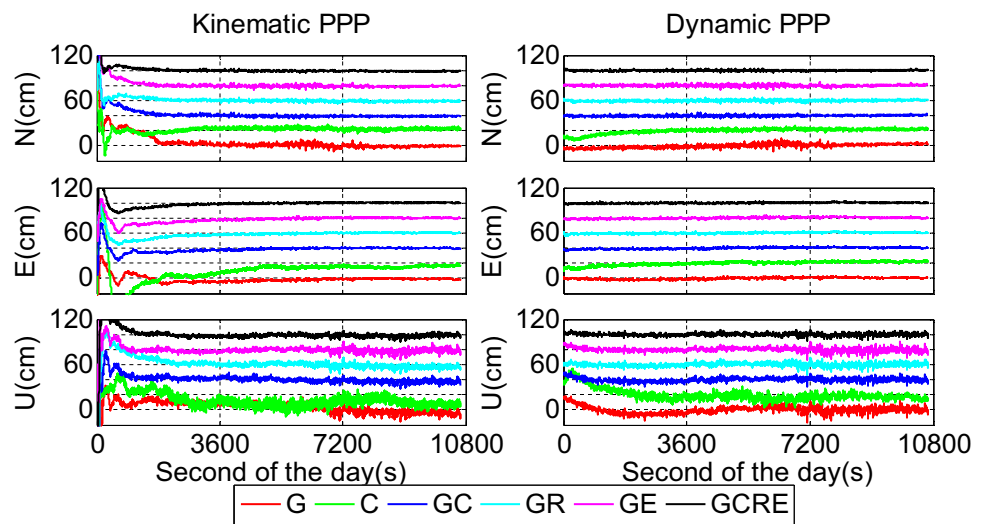

Table 2 RMS statistics of velocity and acceleration errors at JFNG

		G	C	GC	GR	GE	GCRE
Velocity (unit: mm/s)	North	3.281	3.324	2.300	2.776	2.629	2.157
	East	1.922	3.296	1.780	2.102	1.759	1.826
	Up	5.903	7.821	4.467	5.134	5.042	4.098
	3-D	7.022	9.115	5.330	6.203	5.952	4.978
Acceleration (unit: mm/s^2)	North	1.160	1.175	0.999	1.226	1.033	1.049
	East	0.827	1.108	0.804	1.011	0.785	0.922
	Up	1.653	1.598	1.385	1.631	1.488	1.393
	3-D	2.182	2.272	1.888	2.277	1.975	1.972

Table 3 STD statistics of displacement for kinematic and dynamic PPP solution at JFNG

		G	C	GC	GR	GE	GCRE
Kinematic PPP (unit: cm)	North	1.783	1.270	0.751	0.884	1.038	0.590
	East	1.423	2.192	0.967	0.945	1.050	0.671
	Up	5.843	4.745	2.551	2.545	2.543	1.698
	3-D	6.273	5.379	2.829	2.855	2.940	1.919
Dynamic PPP (unit: cm)	North	1.900	1.128	0.826	0.901	1.141	0.607
	East	0.960	1.121	0.769	0.751	0.795	0.581
	Up	3.282	3.585	2.076	2.291	2.681	1.683
	3-D	3.912	3.923	2.363	2.574	3.020	1.881

the GPS-only PDOP values are smaller than Beidou-only cases in some epochs, although the latter possesses more visible satellites. The increased number of satellites can significantly decrease the PDOP values and improve satellite geometry.

The solutions from GPS-only, Beidou-only, GPS + Beidou, GPS + GLONASS, GPS + Galileo, and GPS + Beidou + GLONASS + Galileo utilizing data sets collected at seven stations over 15 consecutive days are compared to further evaluate the performance of the dynamic PPP. Three-hour positioning results are analyzed instead of the daily solutions. A total of 840 sets of results are acquired to get a statistical conclusion. Each session is processed by kinematic PPP and dynamic PPP, respectively. Figure 5 depicts the mean convergence time for all six dynamic PPP solutions in units of seconds utilizing the 840 sets of results. The values of mean convergence time for north, east, and up components are also shown in the figure by different colors. In this study, the convergence solution is defined as the RMS of displacement variations between two adjacent epochs of smaller than 0.01 m and remaining within 0.01 m. The mean convergence time of the
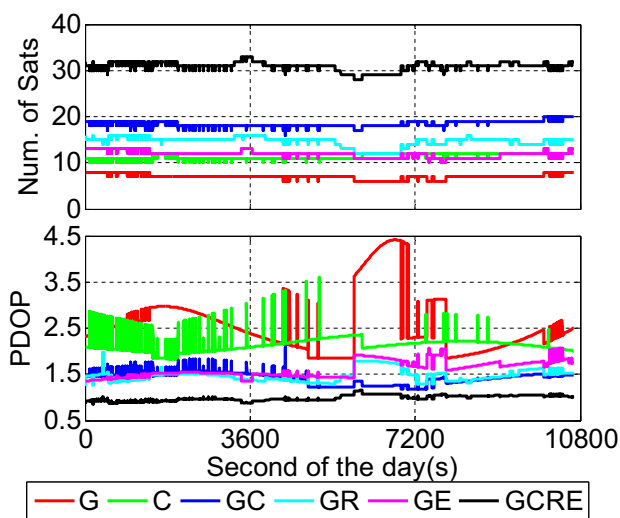
Fig. 4 Number of satellites and PDOP at JFNG

seven stations for GPS-only, Beidou-only, GPS + Beidou, GPS + GLONASS, GPS + Galileo, and quad-constellation dynamic PPP in three directions is 49.4, 104.5, 45.3, 39.9, 47.3, and 35.1 s, respectively.

Figure 6 indicates the average positioning repeatability of the seven stations for GPS-only, Beidou-only, GPS + Beidou, GPS + GLONASS, GPS + Galileo, and GPS + Beidou + GLONASS + Galileo PPP solutions. The kinematic PPP is given for a comparison and values of STDs are also shown in the figure. It is clearly illustrated that Beidou-only dynamic PPP has poorer positioning repeatability than the GPS-only solution. Compared with the GPS-only dynamic PPP, the combination of GPS and Beidou significantly improves the positioning repeatability by 20.8%, 11.8%, and 12.4% in the north, east, and up directions in terms of STD statistics, respectively. For GPS + GLONASS dynamic PPP, the positioning repeatability can be improved by 26.3%, 20.8%, and 13.8%, respectively, in the north, east, and up components. For GPS + Galileo dynamic PPP, the positioning repeatability can be improved by 26.4%, 17.8%, and 21.2%, respectively, in the north, east, and up components.
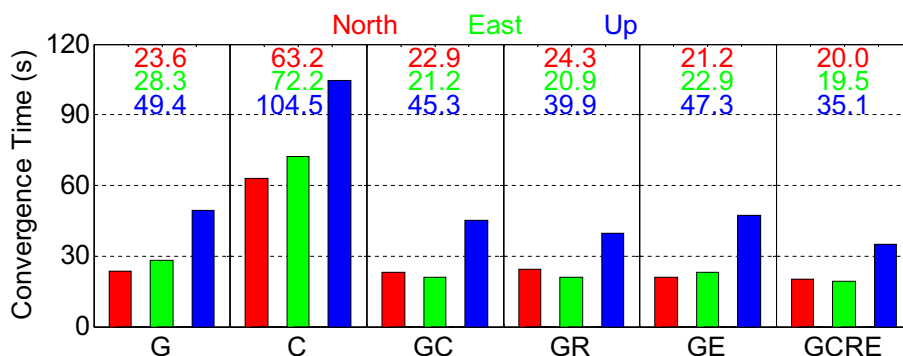
The improvements of the positioning repeatability for quad-constellation dynamic PPP are 35.0%, 26.1%, and 21.5%, respectively, for three components. It is clearly shown that the combinations of multi-GNSS significantly improve the positioning repeatability in the north, east, and up directions.

Application and analysis

We demonstrate the usability of dynamic PPP for kinematic applications in this section. A vehicle-borne kinematic experiment at Beijing and seismic waves capture at station LASA during the 2015 M_w 7.8 Nepal earthquake are conducted.

Vehicle-borne kinematic experiments

For the purpose of application, we investigate the performance of multi-GNSS dynamic PPP on vehicle-borne kinematic positioning. The GNSS data were collected from the vehicle-borne three-dimensional mobile surveying system, while the vehicle was moving. The experiment was conducted in Beijing, China, on March 30, 2018, and the origin of the vehicle was Beijing Foreign Studies University. The system is equipped with a quad-constellation NovAtel GPSCard receiver and inertial measurement unit of span LCI type. The sampling rate of the data is 1 Hz and the cut-off elevation angle is 10°. The data were processed from 09:50 UTC to 12:00 UTC. The trajectory of the experiment is shown in Fig. 7. The same type of receiver of NovAtel GPSCard was set up in Beijing Foreign Studies University as the base station. We used GNSS/INS tightly coupled resolution of Inertial Explorer 8.60 software to handle the data and the results were regarded as an external reference.

Similarly, GPS-only, GPS + Beidou, GPS + GLONASS, and the quad-constellation dynamic PPP solutions are tested with this data set. The acceleration dynamic noises are set to 5 cm s$^{-5/2}$ in this experiment. Figure 8 depicts the positioning errors of GPS-only, GPS + Beidou, GPS + GLONASS, and the quad-constellation dynamic PPP solutions

Fig. 5 Average convergence time of the seven stations for GPS-only, Beidou-only, GPS + Beidou, GPS + GLONASS, GPS + Galileo, and GPS + Beidou + GLONASS + Galileo dynamic PPP solutions. The charts of north, east, and up components are shown by different colors

Fig. 6 Average positioning repeatability of the seven stations for GPS-only, Beidou-only, GPS + Beidou, GPS + GLONASS, GPS + Galileo, and GPS + Beidou + GLONASS + Galileo kinematic PPP and dynamic PPP solutions. The charts of north, east, and up components are shown by different colors
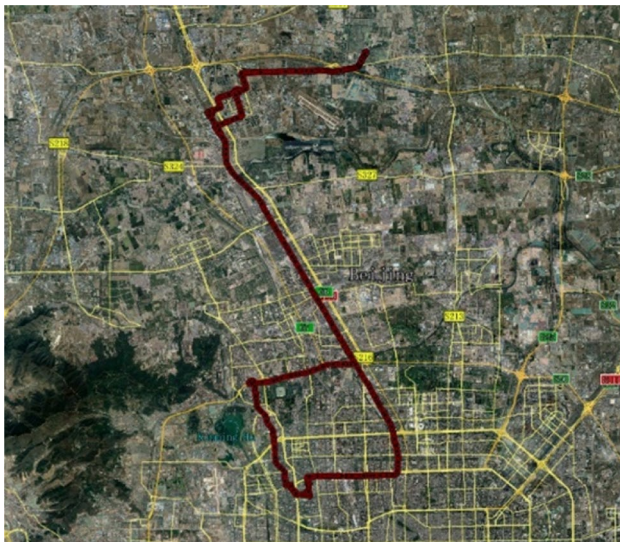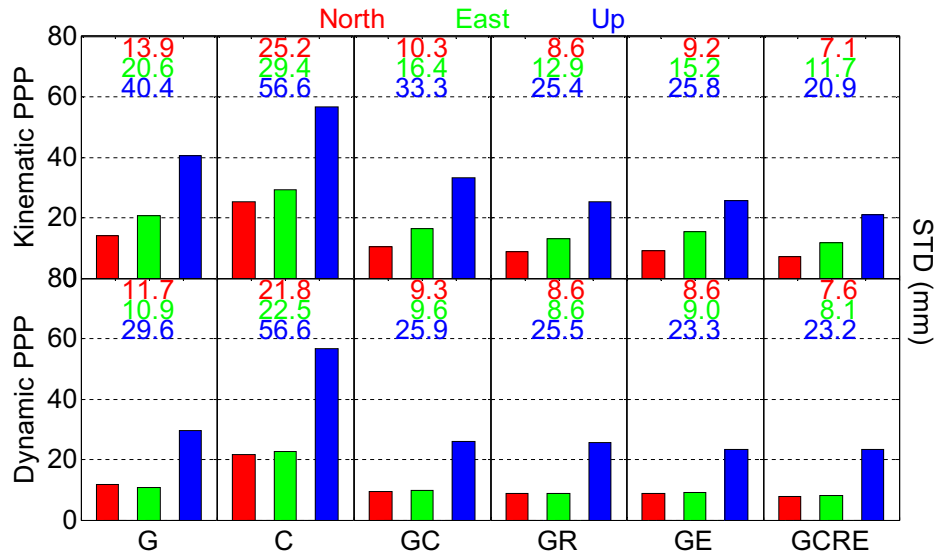

Fig. 7 Trajectory of the vehicle-borne experiment

Fig. 8 Positioning errors of dynamic PPP for GPS-only, GPS + Beidou, GPS + GLONASS and the quad-constellation dynamic PPP solutions

with respect to the reference coordinate values in the north, east, and up components. The results of dynamic PPP solutions with different combinations all have good consistencies with the GNSS/INS tightly coupled resolution results. The positioning precision of the multi-constellation dynamic PPP will be better compared with GPS-only PPP solution. The vertical positioning errors are larger than the horizontal cases for all the processing cases. Figure 9 shows the number of satellites and corresponding PDOP. The number of visible satellites was varied greatly due to building blockage of signals in the city. The average satellite numbers of GPS, Beidou, GLONASS, and Galileo are 9.8, 7.9, 6.5, and 5.9, respectively. The average PDOPs for the four processing cases are 1.97, 1.37, 1.31, and 0.98, respectively.
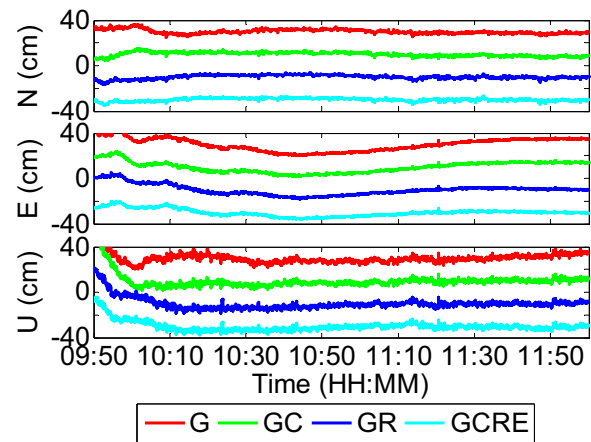
To better assess the precision of dynamic PPP solutions in this experiment, Table 4 provides STD statistics of displacement errors for GPS-only, GPS + Beidou, GPS + GLONASS, and the quad-constellation dynamic PPP solutions. With the combination of GPS and Beidou, the positioning precision is improved by 6.2%, 16.2%, and 7.0% over the GPS-only case for north, east, and up components, respectively. The positioning precision of GPS + GLONASS dynamic PPP is slightly better than the GPS + Beidou solution. With the inclusion of quad-constellation, the dynamic PPP 3-D precision is improved at approximately 4.3 cm compared to the GPS-only solution. Multi-constellation combination can improve the precision of dynamic PPP in the kinematic test. It is demonstrated that dynamic PPP can be applied for
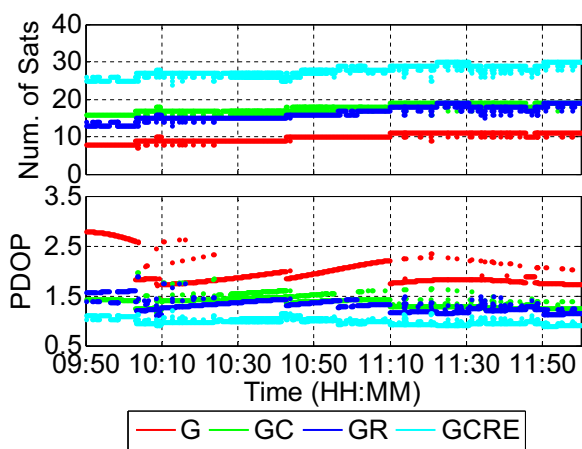
Fig. 9 Number of satellites and PDOP for GPS-only, GPS + Beidou, GPS + GLONASS, and the quad-constellation dynamic PPP solutions

kinematic experiment and does not suffer much convergence time in the kinematic PPP solution.

2015 M_w 7.8 Nepal earthquake

An M_w 7.8 earthquake occurred central Nepal at 06:11:26 UTC on April 25, 2015 at a hypocentral depth of 15 km. The epicenter was located at 28.147°N, 84.708°E, 77 km to the northwest of the Nepalese capital Kathmandu (Wang and Fialko 2015). The earthquake destroyed plenty of houses and buildings, which is the largest and most destructive earthquake since the 1934 Bihar-Nepal earthquake in this region (Bilham 2004; Fan and Shearer 2015).

Station LASA from BETS is capable of recording 1 Hz GPS, Beidou, GLONASS, and Galileo, enabling us to capture seismic waves from multi-GNSS dynamic PPP solution during the earthquake. The strong motion station LSA near Tibet successfully recorded the ground motions induced by the earthquake, which has a sampling rate of 200 Hz and is 5.5 km away from LASA (Geng et al. 2016). We computed the acceleration, velocity, and displacement time series using GPS-only, Beidou-only, GPS + Beidou, GPS + GLONASS, and GPS + Beidou + GLONASS + Galileo measurements,

through dynamic PPP approach collected at LASA. The acceleration dynamic noise is set to 1 cm s$^{-5/2}$ here.

Table 5 provides the STD values of displacements by GPS-only, Beidou-only, GPS + Beidou, GPS + GLONASS, and GPS + Beidou + GLONASS + Galileo dynamic PPP from 5:00 to 6:00, April 25, 2015 (prior to the earthquake event). For GPS-only solution, the STD values of horizontal and vertical components are 1–2 cm and 7.2 cm, respectively. For Beidou-only solution, the horizontal STD is 3–4 cm and the vertical reaches is 7.4 cm, somewhat worse than GPS-only solution. The improvement of GPS + Beidou, GPS + GLONASS, and GPS + Beidou + GLONASS + Galileo dynamic PPP compared with GPS-only solution in 3-D direction is 20.9%, 38.0%, and 42.1%, respectively, which is mainly due to the increased numbers of visible satellites and, thus, better PDOP values.

Figure 10 depicts the acceleration, velocity, and displacement waveforms for north, east, and up components derived from GPS-only, Beidou-only, GPS + Beidou, GPS + GLONASS, and GPS + Beidou + GLONASS + Galileo dynamic PPP solutions at LASA stations for 300 s after the origin time (06:11:26 UTC) of the earthquake. The strong motion station LSA is located closed to station LASA. Velocity waveforms integrated by the accelerometer data after high-pass filtering and displacements obtained through a single integration of velocity of accelerometer data are also shown in the figure. The rotation and tilt of instrument will result in distortion and baseline offsets, showing as a linear or quadratic trend in the displacement time series. The drift of displacements derived from the accelerogram recording is effectively removed from the records (Boore 2001). Compared with strong motion station results, the waveforms derived from dynamic PPP solutions do not suffer the distortion caused by the sensor rotation and tilt inherited in the seismic instruments. The waveforms of LASA station produced from GPS-only, Beidou-only, GPS + Beidou, GPS + GLONASS, and GPS + Beidou + GLONASS + Galileo measurements, and the accelerometer data from station LSA during the earthquake are compared. The results show that there is a high consistency among acceleration, velocity, and displacement waveforms, with similar aligned

Table 4 STD statistics of positioning errors for GPS-only, GPS + Beidou, GPS + GLONASS, and the quad-constellation dynamic PPP solutions

	G	G/C	G/R	G/C/R/E
Precision (unit: cm)				
North	2.007	1.882	1.796	1.365
East	5.821	4.879	4.831	3.267
Up	9.637	8.962	7.298	6.178
3-D	11.436	10.376	8.927	7.112

Table 5 STD statistics of positioning errors at LASA for GPS-only, Beidou-only, GPS + Beidou, GPS + GLONASS, and GPS + Beidou + GLONASS + Galileo dynamic PPP solutions from 5:00 to 6:00, April 25, 2015

	G	C	G/C	G/R	G/C/R/E
Precision (unit: cm)					
North	1.329	3.157	1.291	1.014	0.982
East	2.286	3.857	1.847	1.232	1.280
Up	7.168	7.383	5.610	4.456	4.116
3-D	7.640	8.908	6.045	4.733	4.421

Fig. 10 Acceleration, velocity, and displacement waveforms in north, east, and up components from GPS-only, Beidou-only, GPS + Beidou, GPS + GLO-NASS, and GPS + Bei-dou + GLONASS + Galileo dynamic PPP solutions for 300 s after the origin time (06:11:26 UTC) of the earthquake at LASA and waveforms from strong motion station LSA. The abbreviation ACC represents the strong motion station LSA
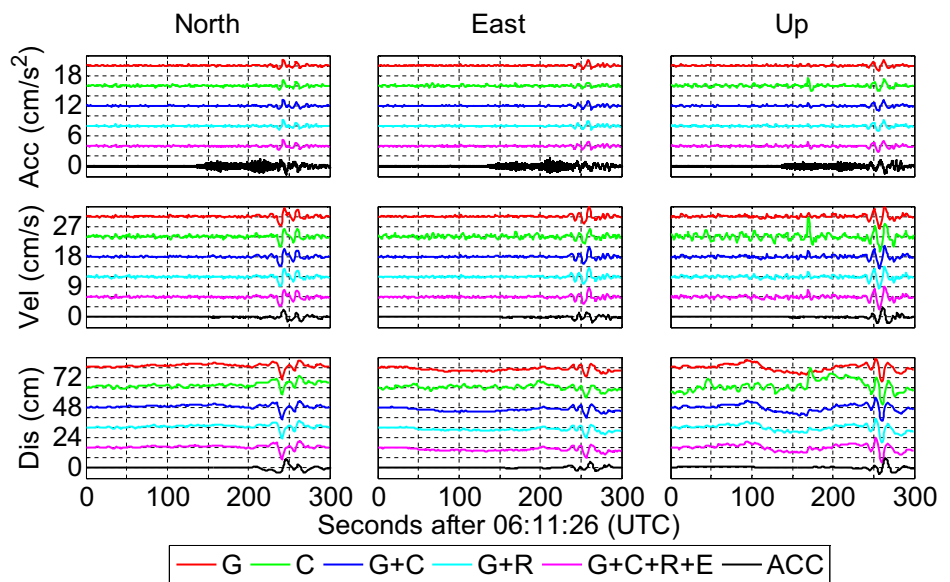
phase and amplitudes in three directions between the GNSS-derived and strong motion results. With the use of more GNSS observations, the displacement waveforms of three components are smoother due to the higher accuracy of acceleration and velocity estimates. The benefits of multi-GNSS dynamic PPP to capture seismic waveforms during the earthquake are demonstrated.

Conclusion

We present a multi-constellation dynamic PPP model for rapid displacement determination with observations from quad-constellations. The model is generally suitable for single-, dual-, triple-, and quad-constellation GNSS data processing. Static datasets collected at seven stations over 15 consecutive days are utilized to evaluate the dynamic PPP model in terms of convergence time and positioning repeatability. Each session with 3-h interval is processed independently, and in total, 840 sets of results are analyzed to derive the conclusions in terms of the convergence time and positioning repeatability.

The dynamic PPP only needs a convergence time of dozens of seconds. The mean convergence time of GPS-only, Beidou-only, GPS + Beidou, GPS + GLONASS, GPS + Galileo, and quad-constellation dynamic PPP is 49.4, 104.5, 45.3, 39.9, 47.3, and 35.1 s, respectively. With respect to the positioning repeatability of dynamic PPP, Beidou-only solution has poorer positioning repeatability than the GPS-only solution. The use of additional constellations will enhance the positioning repeatability of dynamic PPP. Compared with GPS-only PPP, the positioning repeatability of GPS + Beidou solution in the north, east, and up components will improve 20.8%, 11.8%, and 12.4%, respectively. The

improvement for GPS + GLONASS PPP is 26.3%, 20.8%, and 13.8%, respectively, and that for GPS + Galileo PPP is 26.4%, 17.8%, and 21.2%, respectively. The improvement for quad-constellation PPP is 35.0%, 26.1%, and 21.5%, respectively.

The usability of dynamic PPP for kinematic application is also demonstrated. The multi-GNSS dynamic PPP is applied to a vehicle-borne kinematic experiment and to seismic waves capture at station LASA during the 2015 M_w 7.8 Nepal earthquake. The precision of dynamic PPP in the kinematic test will be improved with multi-constellation combination and does not suffer the long convergence time compared to kinematic PPP solution.

References

Bilham R (2004) Earthquakes in India and the Himalaya: tectonics, geodesy and history. Ann Geophys 47(2–3):839–858

Boehm J, Schuh H (2004) Vienna mapping functions in VLBI analyses. Geophys Res Lett 31(1):195–196

Boore DM (2001) Effect of baseline corrections on displacements and response spectra for several recordings of the 1999 Chi–Chi, Taiwan, earthquake. Bullseissocam 91(5):1199–1211

Branzanti M, Colosimo G, Crespi M, Mazzoni A (2013) GPS near-real-time coseismic displacements for the great Tohoku-oki earthquake. IEEE Geosci Remote Sens Lett 10(2):372–376

Colosimo G, Crespi M, Mazzoni A (2011) Real-time GPS seismology with a stand-alone receiver: a preliminary feasibility demonstration. J Geophys Res Solid Earth. https://doi.org/10.1029/2010JB007941

Davis JL, Herring TA, Shapiro II, Rogers AEE, Elgered G (1985) Geodesy by radio interferometry: effects of atmospheric modeling errors on estimates of baseline length. Radio Sci 20(6):1593–1607

Fan W, Shearer PM (2015) Detailed rupture imaging of the 25 April 2015 Nepal earthquake using teleseismic P waves. Geophy Res Lett 42(14):5744–5752

Ge M, Gendt G, Rothacher M, Shi C, Liu J (2008) Resolution of GPS carrier-phase ambiguities in precise point positioning (PPP) with daily observations. J Geod 82(7):389–399

Geng T, Xie X, Fang R, Su X, Zhao Q, Liu G et al (2016) Real-time capture of seismic waves using high-rate multi-GNSS observations: application to the 2015 M_w 7.8 Nepal earthquake. Geophy Res Lett. https://doi.org/10.1002/2015GL067044

Guo F, Zhang X (2014) Real-time clock jump compensation for precise point positioning. GPS Solut 18(1):41–50

Guo H, He H, Li J, Wang A (2011) Estimation and mitigation of the main errors for centimetre-level compass RTK solutions over medium-long baselines. J Navig 64(S1):S113–S126

Guo F, Zhang X, Wang J (2015) Timing group delay and differential code bias corrections for Beidou positioning. J Geod 89(5):427–445

Hopfield HS (1969) Two-quartic tropospheric refractivity profile for correcting satellite data. J Geophys Res 74(18):4487–4499

Jin S, Occhipinti G, Jin R (2015) GNSS ionospheric seismology: recent observation evidence and characteristics. Earth Sci Rev 147:54–64

Jin S, Qian X, Kutoglu H (2016) Snow depth variations estimated from GPS-reflectometry: a case study in Alaska from L2P SNR data. Remote Sens 8(1):63. https://doi.org/10.3390/rs8010063

Kalman RE (1960) A new approach to linear filtering and prediction problems. J Basic Eng Trans 82:35–45

Kouba J (2009) A guide to using international GNSS service (IGS) products. http://igscb.jpl.nasa.gov/igscb/resource/pubs/UsingIGSProductsVer21.pdf

Kouba J, Heroux P (2001) Precise point positioning using IGS orbit and clock products. GPS Solut 5(2):12–28

Lagler K, Schindelegger M, Böhm J, Krásná H, Nilsson T (2013) GPT2: empirical slant delay model for radio space geodetic techniques. Geophy Res Lett 40(6):1069–1073

Lambiel C, Delaloye R (2004) Contribution of real-time kinematic GPS in the study of creeping mountain permafrost: examples from the Western Swiss Alps. Permafrost Periglac Process 15(3):229–241

Leick A, Rapoport L, Tatarnikov D (2015) GPS satellite surveying, 4th edn. Wiley, Hoboken

Li X, Ge M, Zhang Y, Wang R, Xu P, Wickert J, Schuh H (2013) New approach for earthquake/tsunami monitoring using dense GPS networks. Sci Rep 3:2682

Li X, Zhang X, Ren X, Fritsche M, Wickert J, Schuh H (2015) Precise positioning with current multi-constellation global navigation satellite systems: GPS, GLONASS, Galileo and Beidou. Sci Rep 5:8328

Li X, Chen X, Ge M, Schuh H (2018) Improving multi-GNSS ultra-rapid orbit determination for real-time precise point positioning. J Geod 3:1–20

Montenbruck O, Steigenberger P, Khachikyan R, Weber G, Langley RB, Mervart L et al (2014) IGS-MGEX: preparing the ground for multi-constellation GNSS science. Espace 9(1):42–49

Paul W, Nick W, Sally B (2009) GPS jamming and the impact on maritime navigation. J Navig 62(2):173–187

Petit G, Luzum B (eds) (2010) IERS Conventions (2010), IERS Technical Note 36. Verlagdes Bundesamtsfür Kartographie und Geodäsie, Frankfurt am Main, Germany

Rizos C, Montenbruck O, Weber R, Weber G, Neilan R, Hugentobler U (2013) The IGS MGEX experiment as a milestone for a comprehensive multi-GNSS service. In: ION Pacific PNT conference, vol 8900. DLR, pp 289–295

Su K, Jin S (2018) Improvement of multi-GNSS precise point positioning performances with real meteorological data. J Navig 71(6):1363–1380. https://doi.org/10.1017/S0373463318000462

Su K, Jin S, Hoque MM (2019) Evaluation of ionospheric delay effects on multi-GNSS positioning performance. Remote Sens 11(2):171. https://doi.org/10.3390/rs11020171

Tegedor J, Øvstedal O, Vigen E (2014) Precise orbit determination and point positioning using GPS, GLONASS, Galileo and Beidou. J Geod Sci. https://doi.org/10.2478/jogs-2014-0008

Tu R (2013) Fast determination of displacement by PPP velocity estimation. Geophys J Int 196(3):1397–1401. https://doi.org/10.1093/gji/ggt480

Wang K, Fialko Y (2015) Slip model of the 2015 M_w 7.8 Gorkha (Nepal) earthquake from inversions of ALOS-2 and GPS data. Geophys Res Lett 42(18):7452–7458

Wei E, Jin S, Wan L, Liu W, Yang Y, Hu Z (2015) High frequency variations of earth rotation parameters from GPS and GLONASS observations. Sensors 15(2):2944–2963

Wendel J, Meister O, Monikes R, Trommer GF (2006) Time-differenced carrier phase measurements for tightly coupled GPS/INS integration. In: Proceedings of IEEE/ION PLANS 2006, San Diego, CA, April 2006, pp 54–60

Wu JT, Wu SC, Hajj GA, Bertiger WI, Lichten SM (1992) Effects of antenna orientation on GPS carrier phase. Astrodynamics 18:1647–1660) **(Astrodynamics 1991)**

Yang Y, He H, Xu G (2001) Adaptively robust filtering for kinematic geodetic positioning. J Geod 75(2–3):109–116

Yang Y, Li J, Wang A, Xu J, He H, Guo H, Dai X (2014) Preliminary assessment of the navigation and positioning performance of BeiDou regional navigation satellite system. Sci China Earth Sci 57(1):144–152

Zumberge JF, Heflin MB, Jefferson DC, Watkins MM, Webb FH (1997) Precise point positioning for the efficient and robust analysis of GPS data from large networks. J Geophys Res 102(B3):5005–5017. https://doi.org/10.1029/96JB03860

Ke Su is currently working towards the M.Sc. degree with the Shanghai Astronomical Observatory, Chinese Academy of Sciences, Shanghai, China. His research interests include satellite navigation and GNSS seismology.

Shuanggen Jin is a Professor and Group Head at the Shanghai Astronomical Observatory, CAS. His main research areas include satellite navigation, space geodesy, remote sensing, climate change, and space/planetary exploration. He has received 100-Talent Program of CAS, Fellow of IAG, Fellow of IUGG, Member of Russian Academy of Natural Sciences, and Member of European Academy of Sciences.
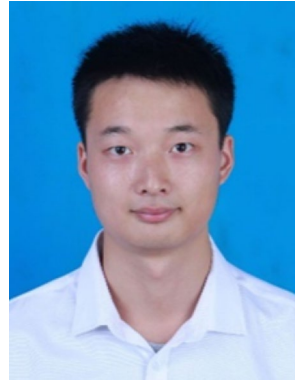
Yulong Ge is currently a Ph.D. student at National Time Service Center, Chinese Academy of Sciences. His current research mainly focuses on multi-constellation and multi-frequency GNSS time transfer.